The growth of typical star-forming galaxies and their supermassive black holes across cosmic time since $z \sim 2$

João Calhau,[1,2]★ David Sobral,[1,2,3] Andra Stroe,[4]† Philip Best,[5] Ian Smail,[6] Bret Lehmer,[7] Chris Harrison[6] and Alasdair Thomson[6]

[1]*Department of Physics, Lancaster University, Lancaster LA1 4YB, UK*
[2]*Instituto de Astrofísica e Ciências do Espaço, Universidade de Lisboa, OAL, Tapada da Ajuda, P-1349-018 Lisboa, Portugal*
[3]*Leiden Observatory, Leiden University, PO Box 9513, NL-2300 RA Leiden, the Netherlands*
[4]*European Southern Observatory, Karl-Schwarzschild-Str. 2, D-85748 Garching, Germany*
[5]*SUPA, Institute for Astronomy, Royal Observatory of Edinburgh, Blackford Hill, Edinburgh EH9 3HJ, UK*
[6]*Centre for Extragalactic Astronomy, Department of Physics, Durham University, South Road, Durham DH1 3LE, UK*
[7]*Department of Physics, University of Arkansas, 226 Physics Building, 835 West Dickson St, Fayetteville, AR 72701, USA*

ABSTRACT

Understanding galaxy formation and evolution requires studying the interplay between the growth of galaxies and the growth of their black holes across cosmic time. Here, we explore a sample of Hα-selected star-forming galaxies from the High Redshift Emission Line Survey and use the wealth of multiwavelength data in the Cosmic Evolution Survey field (X-rays, far-infrared and radio) to study the relative growth rates between typical galaxies and their central supermassive black holes, from $z = 2.23$ to $z = 0$. Typical star-forming galaxies at $z \sim 1$–2 have black hole accretion rates ($\dot{M}_{BH}$) of 0.001–0.01 $M_\odot$ yr^{-1} and star formation rates (SFRs) of $\sim$10–40 $M_\odot$ yr^{-1}, and thus grow their stellar mass much quicker than their black hole mass (3.3±0.2 orders of magnitude faster). However, $\sim$3 per cent of the sample (the sources detected directly in the X-rays) show a significantly quicker growth of the black hole mass (up to 1.5 orders of magnitude quicker growth than the typical sources). $\dot{M}_{BH}$ falls from $z = 2.23$ to $z = 0$, with the decline resembling that of SFR density or the typical SFR (SFR*). We find that the average black hole to galaxy growth ($\dot{M}_{BH}$/SFR) is approximately constant for star-forming galaxies in the last 11 Gyr. The relatively constant $\dot{M}_{BH}$/SFR suggests that these two quantities evolve equivalently through cosmic time and with practically no delay between the two.

Key words: galaxies: evolution – galaxies: high-redshift – galaxies: star formation – cosmology: observations.

1 INTRODUCTION

Understanding how galaxies form and evolve is a very challenging task, as there are a range of complex processes and quantities that need to be taken into account and that usually cannot be studied in isolation, such as gas abundances, dust, supernovae, radiative winds and relativistic jets (e.g. Genel et al. 2014; Schaye et al. 2015). Both the star-formation history (SFH; e.g. Lilly et al. 1996; Karim et al. 2011; Sobral et al. 2013) and the black hole accretion history (BHAH; Brandt & Alexander 2015) are strongly influenced by the feedback effects of both star formation (SF) and black hole (BH) accretion, as they affect the ability of the host galaxy to convert molecular gas into stars. For example, an active galactic

nucleus (AGN) is the result of the accretion of matter into the central supermassive BH of a galaxy. A growing, massive BH releases copious amounts of energy so, provided that there is a strong coupling between radiation and the mechanical output of the BH and surrounding gas, the AGN may be able to disrupt the environment and in principle even quench the SF happening in the host galaxy (e.g. Silk & Rees 1998; Bower et al. 2006). This may happen mainly in two ways: (i) radiatively driven winds and (ii) relativistic jets.

Current studies cannot establish whether or not radiatively driven winds have a significant effect on a galactic scale. Integral field unit observations provide evidence for outflowing gas in local Seyferts (e.g. Davies et al. 2009; Storchi-Bergmann et al. 2010; Schnorr Müller et al. 2011) on scales of 10–100 pc. Conversely, spectropolarimetry of low redshift quasars shows high-velocity outflows close to the accretion disc (e.g. Young et al. 2007; Ganguly & Brotherton 2008). However, these winds are only observed along the line of sight and there are no direct constraints on the distribution

★ E-mail: j.calhau@lancaster.ac.uk
† ESO Fellow.

of the outflowing gas, which makes it difficult to get a clear picture of how they affect the galaxy (e.g. Tremonti, Moustakas & Diamond-Stanic 2007; Dunn et al. 2010; Harrison et al. 2012).

Relativistic jets are known to influence gas on a galactic scale, even reaching outside of the dark matter haloes of galaxies and, in addition, interact strongly with virialized hot atmospheres (e.g. Best et al. 2005; Nesvadba et al. 2006, 2007, 2008; McNamara et al. 2009; McNamara, Rohanizadegan & Nulsen 2011). The accretion of matter into the central BH leads to the emission of radiation from both the accretion disc and the relativistic jets and thus, in conjunction with SF processes and gas dynamics, AGN are thought to be responsible for regulating the evolution of galaxies – but it may well be that AGN feedback mostly works as a maintenance mode (e.g. Best et al. 2005, 2006) rather than be responsible for the actual quenching process.

Stellar feedback also plays a major role in regulating SF. This can happen through extreme events like strong stellar winds or shock waves of supernovae explosions (Geach et al. 2014). Typical outflows from SF involve only small fractions of the molecular gas in Milky Way type galaxies (but are much more important for very low mass galaxies) and thus stellar feedback is generally considered to be insufficient for the regulation without the contribution of an AGN.

In order to understand how galaxies evolve, it is particularly important to understand how key properties such as the star formation rate (SFR) and the BH accretion rate ($\dot{M}_{BH}$) in AGN evolve as a function of cosmic time. This can be done by examining the SF and BHAHs of galaxies. The latest surveys show that SF activity peaks at $z \sim 2$ (e.g. Sobral et al. 2013; Madau & Dickinson 2014) and then declines until today. As for the BH accretion rates, the peak may happen at slightly lower redshifts than the peak of SF, but the BH activity may also decline more rapidly from $z \sim 1$ to 0 (e.g. Aird et al. 2010). However, studies taking into account the bolometric luminosity functions of AGN (e.g. Delvecchio et al. 2014) show that BH accretion tracks the evolution of SF more closely, peaking at $z \sim 2$.

Most studies on the evolution of SF and BH accretion tend to focus on AGN selected samples. Stanley et al. (2015), for example, found that while there is a strong evolution of the average SFR with redshift, the relation between SFR and AGN luminosity seems relatively flat for all redshifts. The authors interpreted this as being due to the effect of short time-scale variations in the mass accretion rates, which might erase any relation that might exist between the SFR and AGN luminosity. Nevertheless, there are also studies with star-forming selected samples: Delvecchio et al. (2015) analysed the relation of AGN accretion and SFR for star-forming galaxies up to $z \sim 2.5$ and found that the ratio between the $\dot{M}_{BH}$ and the SFR evolves slightly with redshift, and has a lower value compared to what one would need to obtain the local M_{BH}–M_{Bulge} relation. Lehmer et al. (2013) also investigated the $\dot{M}_{BH}$/SFR ratio using galaxy samples from both the field and a high-density structure (super-cluster of QSO from the 2QZ survey) at $z \sim 2.23$. Lehmer et al. (2013) found that Hα emitting galaxies in this structure have a relatively high fraction of AGN activity, leading to average $\dot{M}_{BH}$/SFR which are closer to what is typically measured for AGN. For more typical 'field' Hα emitters, the $\dot{M}_{BH}$/SFR was found to be typically an order of magnitude lower than for AGN and for Hα emitters in the higher density region at $z \sim 2$. These results suggest that SF galaxies are generally situated below the local relation (at least at redshifts of $z \sim 2$) and that the activity of the AGN causes the ratio to rise high enough so that the galaxies approach a growth mode that could easily result in the observed local relation. However, much is still unknown, for typical, SF selected samples,

regarding the relative growth of the BH and the host galaxies, and particularly how such relative growth may vary with time, from the peak of the SFH, at $z \sim 2.5$ to $z \sim 0$.

In this paper, we explore a sample of 'typical' star-forming galaxies from High Redshift Emission Line Survey (HiZELS) in the Cosmic Evolution Survey (COSMOS) field, selected in four different redshift slices in a self-consistent, homogenous way. We explore the wealth and variety of exquisite data in the COSMOS field to study the relative growth between the central BHs and their host galaxies, and how that varies across cosmic time. This paper is organized as follows: Section 2 presents the data and sample. Section 3 provides an overview of our selection of potential AGNs. Section 4 presents our stacking analysis in different bands. Section 5 presents the results: the relative supermassive BH/galaxy growth and in Section 6 we present the conclusions. In this paper, we use a Chabrier initial mass function (IMF; Chabrier 2003) and the following cosmology: $H_0 = 70$ km s^{-1} Mpc^{-1}, $\Omega_M = 0.3$ and $\Omega_\Lambda = 0.7$.

2 DATA AND SAMPLE

2.1 Data: X-rays, radio and FIR

2.1.1 X-rays: C-COSMOS

The *Chandra* Cosmos Survey (C-COSMOS; Elvis et al. 2009; Puccetti et al. 2009) imaged the COSMOS field (Scoville et al. 2007) with an effective exposure time of ∼180 ks and a resolution of 0.5 arcsec. The limiting source detection depths are 1.9×10^{-16} erg s^{-1} cm^{-2} in the soft band (0.5–2 keV), 7.3×10^{-16} erg s^{-1} cm^{-2} in the hard band (2–10 keV) and 5.7×10^{-16} erg s^{-1} cm^{-2} in the full band (0.5–10 keV). The data allows us to track X-ray emission from processes like Bremsstrahlung and inverse-Compton scattering, and thus to identify which sources are AGN based on their X-ray emission. C-COSMOS only covers the relatively central area of COSMOS (0.9 deg^2), and thus we restrict our analysis to that region.

2.1.2 Radio: VLA-COSMOS

The VLA-COSMOS Survey (Schinnerer et al. 2004, 2007; Bondi et al. 2008) used the National Radio Astronomy Observatory's very large array (VLA) to conduct deep ($\sigma_{1.4} \sim 10$ μJy beam^{-1}), wide-field imaging with ≈1.5 arcsec resolution at 1.4 GHz continuum of the two square-degree COSMOS field. With this band, we track the radio emission of AGN via synchrotron radiation from supermassive black hole (SMBH) relativistic jets and estimate SFRs from the synchrotron radiation due to supernovae explosions (Schmitt et al. 2006).

2.1.3 Far-infrared: Herschel

COSMOS was imaged with the *Herschel* telescope as part of the *Herschel* Multi-tiered Extragalactic Survey (HerMES; Oliver et al. 2012). HerMES is a legacy programme that mapped 380 deg^2 of the sky – *Herschel*-SPIRE (250, 350 and 500 μm, with a PSF FWHM of 18.1, 24.9 and 36.6 arcsec, respectively; Griffin et al. 2010). We additionally make use of the *Herschel* PACS Evolutionary Probe programme (PEP: 100 and 160 μm, with PSFs of 7.2 and 12 arcsec; Lutz et al. 2011) and the observations of the Submillimetre Common-User Bolometer Array 2 (SCUBA2) on the James Clerk Maxwell Telescope, at 850 μm, for the COSMOS Legacy Survey (Geach et al. 2013, 2016). These bands cover the peak of the redshifted thermal spectral energy distribution from interstellar dust for

galaxies in the redshift range ($z \sim 0.4$–2.2) for the entire COSMOS field. The bands therefore capture optical and UV radiation that has been absorbed and re-emitted by dust.

2.2 The sample of Hα emitters at $z = 0.4$–2.23

HiZELS (Geach et al. 2008; Sobral et al. 2009a,b, 2012, 2013; Best et al. 2013) has surveyed some of the best-studied extragalactic fields for Hα emitters at various narrow redshift ranges, from $z = 0.4$ to $z = 2.23$ (see Sobral et al. 2013). HiZELS used a set of narrow-band filters in the near-infrared J, H and K bands and the Wide Field CAMera (Casali et al. 2007) on the United Kingdom Infrared Telescope, coupled with a filter in the z' band (NB921; Sobral et al. 2012, 2013) mounted on Suprime-cam on the Subaru telescope, to cover roughly 5 deg^2 of extragalactic sky. While it is true that using only Hα as a tracer for SF may cause us to miss obscured SF, the use of bluer bands for the detection of star-forming galaxies (UV or bluer emission lines) would result in missing a much more significant part of the population. In addition, Oteo et al. (2015) showed that an Hα selection is able to recover $\sim$100 per cent of star-forming galaxies (including the most dusty ones), and *Herschel* is then ideal to recover the full SFRs of such highly obscured galaxies (e.g. Ibar et al. 2013). Although HiZELS covers various fields, in this work we focus only on the COSMOS field due to the availability of deep data from the *Chandra* Observatory, on which we rely in order to measure the X-ray luminosities in our samples. HiZELS obtained large samples of Hα-selected galaxies at redshifts $z = 0.4$, $z = 0.84$, $z = 1.47$ and $z = 2.23$ in the COSMOS and UKIDSS Ultra Deep Survey fields (Sobral et al. 2013). The Hα emitters were selected using a combination of broad-band colours (colour–colour selections) and photometric redshifts. Spectroscopically confirmed sources are included in the sample and the sources confirmed to be other emission line emitters are removed. We refer the interested reader to Sobral et al. (2013) for the detailed explanation of the process of selection for the Hα emitters. Furthermore, we note that while the HiZELS sample at $z = 0.4$ (obtained with the Subaru telescope) probes down to significantly lower Hα luminosities and stellar masses (see Sobral et al. 2014) than those at higher redshift, it also covers a significantly smaller volume, and thus misses massive, bright sources (see Fig. 1). In an attempt to make the $z = 0.4$ sample more comparable to those at higher redshift, we apply a mass cut of $M > 10^9$ M$_\odot$. As we will rely on *Chandra* data for deep X-ray data (Section 2.1.1), we also need to restrict our analysis to the area in COSMOS with deep *Chandra* coverage. Thus, our final sample is composed of 35, 224, 137 and 276 Hα emitters at $z = 0.40$, $z = 0.84$, $z = 1.47$ and $z = 2.23$. These are the sources restricted by *Chandra* coverage but include both the ones detected in the C-COSMOS survey and the ones without detectable X-ray emission. We present the distribution of Hα (observed luminosities) in Fig. 1.

3 AGN SELECTION

3.1 X-ray detections

X-rays are one of the best ways to search for AGN. As matter falls into the BH, it heats up, leading to the emission of radiation in the X-rays through inverse-Compton scattering of UV emission coming from the accretion disc. As the X-ray luminosity is expected to scale with the accretion rate, we can use X-ray luminosities to not only identify AGN, but also to obtain an estimate of the SMBH growth rates.
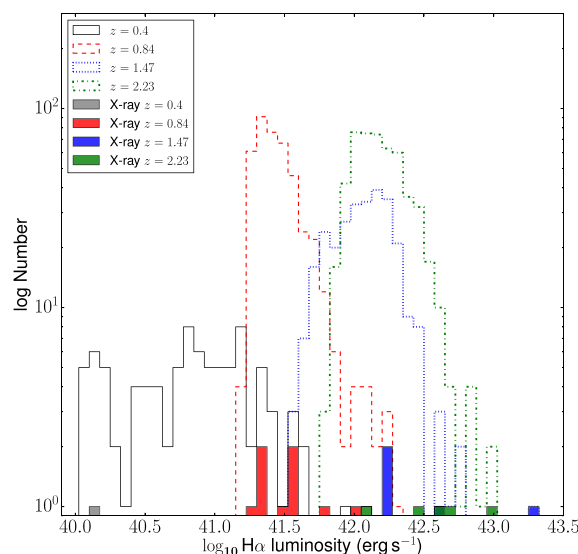
Figure 1. Hα luminosity distribution of the sample of Hα emitters that are used in this paper (after the application of a stellar mass cut, see Section 2.2) and those with individually detected X-ray emission (filled histograms). X-ray detected Hα emitters have 'typical' to high Hα luminosities. Note that the $z = 0.40$ sample covers a much smaller volume than those at higher redshift, thus missing luminous and rarer sources.

Table 1. The luminosity in the X-rays and central $\dot{M}_{BH}$ for the sources directly detected by the C-COSMOS survey (all sources directly detected have luminosities higher than 10^{41} erg s^{-1}).

Source ID* (S13)	Redshift	$\log_{10} L_X$ (erg s^{-1})	$\dot{M}_{BH}$ (M$_\odot$ yr^{-1})
S12-93079	0.40	41.97 ± 0.09	0.003 ± 0.0008
S12-22675	0.84	43.32 ± 0.04	0.074 ± 0.008
S12-33061	0.84	43.77 ± 0.03	0.207 ± 0.016
S12-26956	0.84	43.89 ± 0.03	0.273 ± 0.02
S12-11275	0.84	42.76 ± 0.09	0.02 ± 0.004
S12-6454	0.84	42.85 ± 0.07	0.024 ± 0.005
S12-4541	0.84	42.96 ± 0.08	0.032 ± 0.007
S12-2436	0.84	42.69 ± 0.14	0.017 ± 0.006
S12-23041	1.47	43.93 ± 0.04	0.3 ± 0.032
S12-19279	1.47	44.88 ± 0.01	2.69 ± 0.074
S12-20593	1.47	43.40 ± 0.07	0.087 ± 0.016
S12-44372	1.47	42.96 ± 0.14	0.032 ± 0.013
S12B-1528	2.23	43.67 ± 0.08	0.16 ± 0.033
S12B-1073	2.23	43.48 ± 0.11	0.106 ± 0.032
S12B-9274	2.23	43.66 ± 0.10	0.098 ± 0.042
S12B-1139	2.23	43.38 ± 0.14	0.085 ± 0.032
S12B-2306	2.23	43.45 ± 0.13	0.1 ± 0.035

*These sources were taken directly from the tables of the HiZELS survey. In order to get the HiZELS designation for each galaxy, one should add 'HiZELS-COSMOS-NB# DTC' to the beginning of the source's name, where # stands for the number or letter identifying the filter.

We cross-correlate our sample of Hα emitters with the *Chandra* X-ray catalogue with a 1 arcsec matching radius, in order to find which of our sources are directly detected in the X-rays and thus likely AGN. We find one direct detection at $z = 0.4$ (2.9 ± 1.7 per cent of the total sample at this redshift), seven at $z = 0.84$ (3.1 ± 1.8 per cent), four at $z = 1.47$ (2.9 ± 1.7 per cent) and five at $z = 2.23$ (1.8 ± 1.3 per cent) in the C-COSMOS catalogue. The results are presented in Table 1. The directly detected sources possess X-ray luminosities of the order of $\geq 10^{42}$ erg s^{-1}, which are typical

Table 2. Quantities estimated for the stacked sources. Fluxes and luminosities in the X-ray band and estimated BH accretion rates from these quantities were estimated from C-COSMOS. SFR estimated from the FIR luminosities as determined by Thomson et al. (2016) and from radio data from VLA-COSMOS.

Source ID/filter	z	log Flux (X-rays) (erg s^{-1} cm^{-2})	log Luminosity (X-rays) (erg s^{-1})	log Luminosity IR (FIR) (L$_\odot$)	SFR (FIR) (M$_\odot$ yr^{-1})	SFR (Radio) (M$_\odot$ yr^{-1})	$\dot{M}_{BH}$ (M$_\odot$ yr^{-1})	log [$\dot{M}_{BH}$/SFR] (FIR) (X-rays)
NB921	0.4	< -15.4	<41.25	10.4 ± 0.26	$2^{+1.6}_{-0.9}$	$1.5^{+0.5}_{-0.2}$	<0.0006	<-3.55
NBJ	0.85	-15.26 ± 0.12	42.12 ± 0.12	11.1 ± 0.23	$13^{+8.8}_{-5.2}$	$10.5^{+0.7}_{-0.6}$	0.004 ± 0.001	-3.51 ± 0.3
NBH	1.47	-15.06 ± 0.07	42.83 ± 0.07	11.5 ± 0.23	$32^{+21.7}_{-13.4}$	$62^{+3}_{-2.7}$	0.02 ± 0.004	-3.20 ± 0.28
NBK	2.23	-15.33 ± 0.12	42.94 ± 0.12	11.6 ± 0.42	$40^{+64.7}_{-24.9}$	$21^{+1.4}_{-1.3}$	0.03 ± 0.01	-3.10 ± 0.3

Table 3. Number of Hα emitters classified as possible and likely AGN according to the selections mentioned in Section 3.

Method	$z = 0.4$	$z = 0.84$	$z = 1.47$	$z = 2.23$	Total
X-ray counterpart (C-COSMOS)	1	7	4	5	18
X-ray AGN fraction	3 ± 2 per cent	3 ± 2 per cent	3 ± 2 per cent	2 ± 1 per cent	3 ± 2 per cent
Radio counterpart (VLA-COSMOS)	1	11	7	9	28
Sources retained for stacking (X-rays)	35	224	137	276	672
Sources retained for stacking (radio)	35	214	132	268	649
Sources retained for stacking (FIR)	35	224	136	276	671

of the luminosities expected from AGN in this band. Our results are consistent with a non-evolving fraction of X-ray AGN within Hα selected samples over the last 11 Gyr of cosmic time (since $z \sim 2.2$), although we have low number statistics (see Table 2). In Fig. 1 we present the Hα luminosity distribution of the directly detected AGN, finding that they have preferentially higher than average Hα luminosities, raising the possibility that our sources might be contaminated in the Hα by AGN.

3.2 Radio detections

We cross-correlated the VLA-COSMOS deep catalogue with our Hα emitters. Our match between the VLA-COSMOS and our sources resulted in: (i) 1 source is detected at $z = 0.4$ (2.9 ± 1.7 per cent), 11 radio sources for $z = 0.84$ (4.9 ± 2.2 per cent), 7 sources for $z = 1.47$ (5.1 ± 2.3 per cent) and 9 for $z = 2.23$ (3.3 ± 1.8 per cent). We estimated the radio luminosities by using:

$$L_{1.4GHz} = 4\pi d_L^2 S_{1.4GHz} 10^{-33}(1+z)^{\alpha-1} \, (\text{W Hz}^{-1}), \tag{1}$$

where d_L is the luminosity distance (in cm), $S_{1.4GHz}$ is the flux density in mJy and α is the radio spectral index – assumed to be 0.8, the characteristic spectral index of synchrotron radiation. 0.8 is a good average value for SF-dominated galaxies (e.g. Thomson et al. 2014), although it is not clear if this value is the best choice if the sample contains a large quantity of AGN. Our SF-selected sample should not have too many AGN (see Table 3) so $\alpha = 0.8$ should be appropriate. Within our Hα emitters, the radio sources have radio luminosities of the order of $\sim 10^{21}$ W Hz^{-1} at $z = 0.40$, $\sim 10^{23}$ W Hz^{-1} for $z = 0.84$–2.23. It is possible for radio detect up emission from a population of supernova remnants as well. However, the emission from these sources have lower luminosity than the AGN we are tracing and should not contaminate the measurements.

4 STACKING ANALYSIS: $\dot{M}_{BH}$ AND SFR

4.1 Radio stacking: SFR

After rejecting all strong radio sources within our Hα selected samples, we can stack the remaining sources, and use radio luminosities
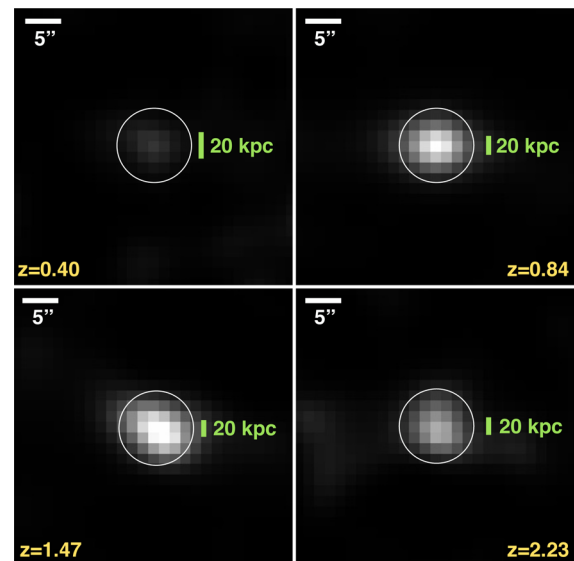
Figure 2. Stacking in the radio (1.4 GHz) for our non-radio AGN sources, at each redshift. We find strong detections at every redshift with luminosities of $\approx 10^{21-23}$ W Hz^{-1}, corresponding to SFRs of $\sim$1.5–63 M$_\odot$. The images were smoothed for easier inspection.

as a dust-free SF indicator (although some contribution of lower luminosity AGN will still be present, thus likely biasing results towards high SFRs). We follow the same stacking procedure as for our X-ray stacking (see Section 4.3) and find high signal-to-noise (S/N) detections of our mean radio stacks in every redshift (see Fig. 2). We find radio luminosities of 4.6×10^{21}, 3.3×10^{22}, 2.0×10^{23} and 1.0×10^{23} W Hz^{-1} for $z = 0.4$, 0.84, 1.47 and 2.23, respectively.

To convert the luminosities to SFR, we adopted the conversion determined by Yun, Reddy & Condon (2001) converted to a Chabrier IMF (e.g. Karim et al. 2011):

$$SFR_{1.4GHz} = 3.18 \times 10^{-22} L_{1.4GHz} \, (\text{M}_\odot \text{ yr}^{-1}). \tag{2}$$

The conversion is suitable for radio luminosities up to, and including, 10^{24} W Hz^{-1} and thus expected to yield reasonable results. We find SFRs of $\approx$1.5, 10.5, 62 and 21 M$_\odot$ yr^{-1} at $z = 0.4$, 0.84, 1.47 and 2.23, respectively.

4.2 FIR stacking: SFRs

When estimating the SFR, it is important to make sure that there is no contamination to the luminosities by the activity of the AGN. Far-infrared (FIR) emission from the cold dust (rest frame 40–500 μm: Rowan-Robinson 1995; Schweitzer et al. 2006; Netzer et al. 2007) should have little to no such contamination.

Cross-correlating our sample with the HerMES catalogue with a 1 arcsec matching radius resulted in 2 sources being directly detected for $z = 0.4$, 10 for $z = 0.84$, 5 for $z = 1.47$ and 7 galaxies directly detected for $z = 2.23$ (see also Ibar et al. 2013; Oteo et al. 2015). As expected, most of the sample, made of much more 'typical' star-forming galaxies, is below the depth of *Herschel*, or SCUBA2, in COSMOS. However, by the means of stacking, one can reach much lower flux limits, and thus detect the mean star-forming galaxy at each redshift. In order to obtain the necessary SFRs, we make use of the results achieved by Thomson et al. (2016). The stacks were obtained through mean statistics accounting for background emission and confusion noise. Aperture corrections were applied for the PACS 100 and 160 μm bands, as specified in the PACS PEP release notes. In the SPIRE 250, 350 and 500 μm, the fluxes were taken from the peak value in each stack. The IR luminosities were then estimated by fitting modified blackbody (grey-body) templates to the data points and integrating the best fit between 100 and 850 μm (see Fig. A1). We refer the interested reader to Thomson et al. (2016) for the description of the complete procedure.

We use the total FIR luminosity to compute SFRs (Chabrier IMF) by using:

$$\text{SFR} = L_{\text{IR}} \times 2.5 \times 10^{-44} \ (\text{M}_\odot \text{yr}^{-1}). \tag{3}$$

This translates to a SFR ranging from 2 to 38 M$_\odot$ yr^{-1} at $z = 0.4$–2.23 (see Table 2).

4.3 X-ray stacking

The vast majority of our Hα emitters ($\sim$98 per cent) are undetected in the X-rays for the current C-COSMOS flux limit. This is expected given that the *Chandra* sensitivity limit is $>10^{-16}$ erg s^{-1} cm^{-2}. Thus, only relatively luminous AGN are expected to be X-ray detected, while our sample is strongly dominated by typical star-forming galaxies. However, we can rely on stacking in order to study the overall population of typical Hα selected galaxies below the X-ray detection limit and recover much lower BH accretion activity. In order to stack our samples of Hα emitters, per redshift, we use the full energy band of C-COSMOS (0.5–7 keV) and start by cutting-out a square of 10 arcsec $\times$ 10 arcsec centred on each source. We adopt a stacking radius of 2 arcsec (the area radius from which we extract the counts for the fluxes). These values were obtained by going through different values for the radius, selecting the ones that maximized the S/N ratio (see Lehmer et al. 2007 for details) and taking the mean. When stacking, we use all sources (both detected and non-detected), allowing us to include the entire population. *Chandra*'s PSF changes with the distance to the pointings, causing deformation of sources. However, the effect of the changing PSF is minimal when compared with the error bars and uncertainties inherent to the FIR analysis. As such we did not apply a correction
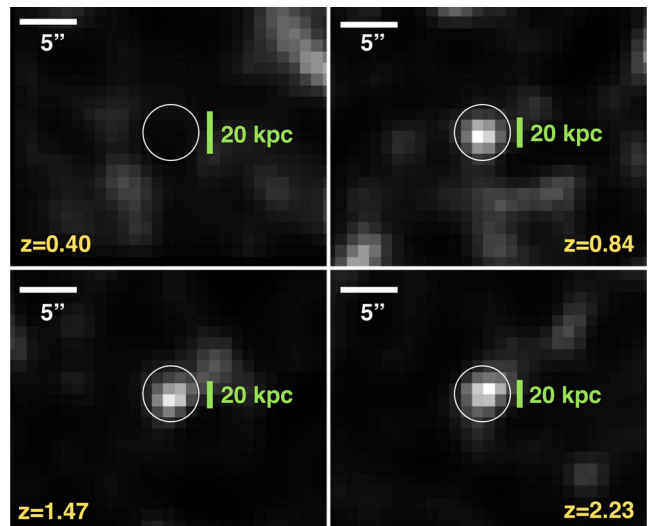
Figure 3. Stacking in the X-rays (*Chandra*'s full band) for all our Hα sources within the C-COSMOS coverage, in each our redshifts slices. The results show high S/N detections at every redshift except for $z = 0.4$. It is worth noting, however, that the sample at $z = 0.4$ is much smaller and has much lower stellar mass and SFR on average than the other redshifts considered, and fails to encompass the rare luminous objects like AGN (see Fig. 1), since it comes from a much smaller volume than the samples at higher redshifts. The images in this figure have been smoothed for easier inspection.

to this effect and instead estimated the background contribution by taking the standard deviation of the pixel counts in a randomized number of areas of the same size of the stacking area, making sure these would fall outside the vicinity of the stacking radius, in order to counter the possible presence of sources distorted by the changes in *Chandra*'s PSF.

To convert background subtracted counts into fluxes, we divided them by the mean exposure time multiplied by the conversion factor (CR $\times 10^{-11}$ erg cm^{-2} s^{-1} (counts s^{-1})$^{-1}$, where CR is the count rate) assuming a power law of photon index $\Gamma = 1.4$ and a Galactic absorption $N_{\text{H}} = 2.7 \times 10^{20}$ as in Elvis et al. (2009). A photon index of 1.4 is appropriate for faint galaxies (see Alexander et al. 2003), as we expect star-forming galaxies to be. Finally, all images were background subtracted. The estimation of the luminosities was done following:

$$L_{\text{X}} = 4\pi d_{\text{L}}^2 f_{\text{X}} (1+z)^{\Gamma - 2} \ (\text{erg s}^{-1}), \tag{4}$$

where d_{L} is the luminosity distance, f_{X} is the flux in the X-ray band, z is the redshift and Γ is the photon index, assumed to be 1.4.

Fig. 3 shows the results of the stacking for the four redshifts. There are clear detections for $z = 0.84$, $z = 1.47$ and $z = 2.23$. For $z = 0.4$ the S/N is much lower. This is not surprising, as (i) this is the smallest sample and particularly because (ii) the sources in the $z = 0.4$ (due to the much smaller volume probed, see Section 2.2) are typically much lower luminosity and have lower stellar masses than those at higher redshift.

4.3.1 Black hole accretion rate from X-ray luminosity

We use the X-ray luminosity to estimate the rate at which the supermassive BH at the centre of galaxies is accreting matter:

$$\dot{M}_{\text{BH}} = \frac{(1-\epsilon)L_{\text{bol}}^{\text{AGN}}}{\epsilon c^2} (\text{M}_\odot \text{ yr}^{-1}), \tag{5}$$
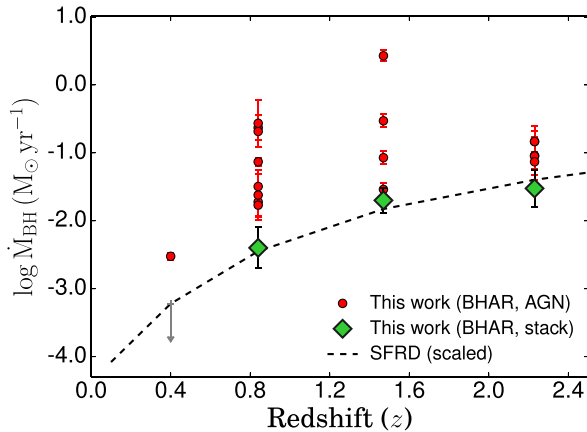
Figure 4. The evolution of BH accretion rates ($\dot{M}_{BH}$), for individually detected (in the X-rays) AGNs and for the stacks of the full samples. We compare those with a scaled evolution of the SFR density, SFRD (Sobral et al. 2013). The SFRD has been scaled to coincide with the $\dot{M}_{BH}$ at $z = 0.4$. The results show that the $\dot{M}_{BH}$ grows with redshift, starting to plateau at z $\sim$ 2.23 and that the SFRD evolves in a very similar way to the accretion rate of the BHs, starting to stabilize at around the same redshifts. The grey down arrow represents a non-detection for the $z = 0.4$ stack.

where $\dot{M}_{BH}$ is the accretion rate of the BH, ϵ is the accretion efficiency, L_{bol}^{AGN} is the bolometric luminosity of the AGN, obtained by multiplying the X-ray luminosity by 22.4 (Vasudevan & Fabian 2007; Lehmer et al. 2013), and c is the speed of light. We find that our typical star-forming galaxies have accretion rates that rise with increasing redshift, from $\approx$0.004 M$_\odot$ yr^{-1} at $z = 0.84$ to $\approx$0.03 M$_\odot$ yr^{-1} at $z = 2.23$. When extracting the accretion rates from the X-ray luminosities, we estimated the correction that would have to be taken into account from the contribution to the X-ray emission by SF. This correction was estimated following Lehmer et al. (2016):

$$\log L_X = A + B \log(SFR) + C \log(1 + z) \quad (6)$$

where A, B and C have the values 39.82 ± 0.05, 0.63 ± 0.04 and 1.31 ± 0.11, respectively. The correction turned out to be at most $\sim$0.05 per cent of the total BH accretion, much less than the uncertainties in quantities like SFR and actual black hole accretion rate (BHAR) and, as such, we do not take it into account. It also seems to evolve with galactic stellar mass, growing as the mass grows and following $L_X = 1.44(SFR) - 0.45$ with $\chi^2 = 1.8$ when fitted to a linear relation through the least-squares method. This evolution of the contribution to the X-rays from stars is not surprising, as the SFR also grows with stellar mass (see Section 5.2 and Fig. B1).

5 RESULTS

5.1 The cosmic evolution of black hole accretion rates

We find that $\dot{M}_{BH}$ rises with increasing redshift as shown in Fig. 4. However, from $z = 1.47$ to $z = 2.23$, even though the accretion rate still rises, it does so less steeply. This is consistent with the results in the literature: Aird et al. (2010) finds the peak of AGN luminosity density to be at $z = 1.2 \pm 0.1$. We compare this redshift evolution with the evolution of the SFR density, also shown in Fig. 4. We use the results from Sobral et al. (2013, 2014) and scale them arbitrarily to look for any potential differences and/or similarities between the evolution of SFRD and $\dot{M}_{BH}$ across cosmic time. Our scaling clearly reveals that star-forming galaxies form stars at a much higher rate
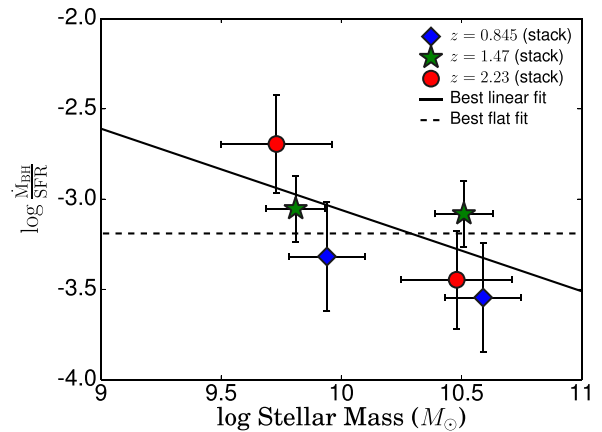
Figure 5. The BH accretion rate/SFR ratio ($\dot{M}_{BH}$/SFR) versus stellar mass for typical star-forming galaxies. The $\dot{M}_{BH}$/SFR ratio seems to generally decrease with stellar mass, indicating that more massive star-forming galaxies grow faster than their BHs compared to the least massive ones. The solid black line represents the best linear fit for [log($\dot{M}_{BH}$/SFR) = $-0.45 \log(M) + 1.44$; reduced $\chi^2 = 1.8$]. The dashed line represents the best fit for a flat relation (reduced $\chi^2 = 2.8$).

than they grow their BHs ($\sim$3.3 orders of magnitude faster), but the relative evolution seems to be the same across redshift. We explore this further in Section 5.3. We also show the accretion rates computed for each individual X-ray AGN, which reveal large scatter (likely due to the high variability of AGN), but that generally agree with the trend of the global population.

5.2 The dependence of $\dot{M}_{BH}$/SFR on stellar mass

Using the results from the FIR analysis, we are able to estimate SFRs which should be independent of AGN activity. We use those to determine the ratio between the BH accretion rate and SFR ($\dot{M}_{BH}$/SFR). Fig. 5 shows how $\dot{M}_{BH}$/SFR depends on stellar mass (stellar masses computed in Sobral et al. 2014) for the three different redshifts where we can easily split our samples. We find that a linear relation with a slope of -0.45 provides the best fit (see Fig. 5). We find that both $\dot{M}_{BH}$ and SFR increase with stellar mass, but SFR seems to rise slightly faster with stellar mass than $\dot{M}_{BH}$ (see Fig. B1). However, our results are still fully consistent with a completely flat relation (only $\sim$1σ away from a flat relation). This may be a sign that the BH accretion and SF of our typical star-forming galaxies evolve at equivalent rates across cosmic time, as we do not find any strong evidence for evolution with cosmic time either. Given that the peak of BH and SF activity is thought to occur at redshifts between $z \sim 1$ and $z \sim 2$, this constancy seems to support the idea that the central supermassive BHs and SF mechanism form a single way of regulating galaxy growth, as opposed to one mechanism taking over the other at set intervals in time. It should be noted, however, that other works, such as Kormendy & Ho (2013) and Rodighiero et al. (2015), have found a different evolution of the ratio with stellar mass with the ratio increasing with the stellar mass, with Rodighiero et al. (2015) finding that the ratio between the X-ray luminosity and SFR scales as log (L_X/SFR) $\propto M_*^{0.43\pm0.09}$.

5.3 Relative black hole-galaxy growth and its redshift evolution

Fig. 6 shows how the ratio between the BH accretion rate and SFR evolves across cosmic time (see also Table 2). We find that the ratio between BH and galaxy growth is very low and is surprisingly
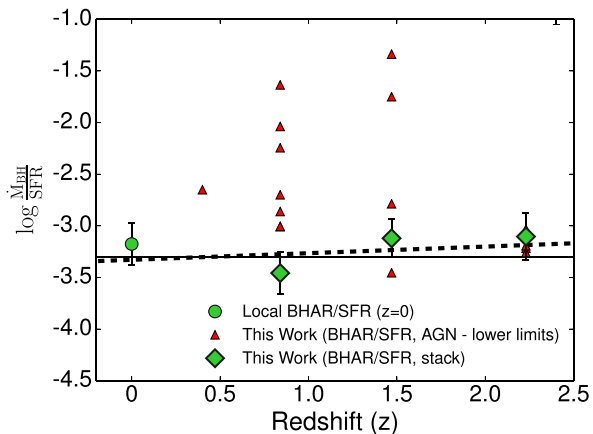
Figure 6. The evolution of the BH accretion rate/SFR ratio ($\dot{M}_{\rm BH}$/SFR) from $z = 0$ to $z = 2.23$. Our results show little to no evolution in $\dot{M}_{\rm BH}$/SFR over the last 11 Gyr of cosmic time. The grey line represents a constant relation, while the dashed line is the best fit (less than 1σ away from a flat relation). The ratio for the stacking remains approximately the same for all redshifts (-3.3 ± 0.2), being consistent with the measured $\dot{M}_{\rm BH}$/SFR value for the local Universe. This seems to show that typical star-forming galaxies form stars much faster than their BHs grow, with such difference being approximately constant across cosmic time. We also show lower limits for individual sources detected in the X-rays there; these show a large scatter with a potential peak at $z \sim 1$–1.5.

constant across redshift, $\sim 10^{-3.3}$. We thus find little to no evolution from $z = 2.23$ to $z = 0$. We investigate a potential linear fit and compare it to a flat relation (no evolution in redshift). Our results prefer a slope that is completely consistent, within less than 1σ with a flat relation (see Fig. 6). This is consistent with previous results: Mullaney et al. (2012) find a flat, non-evolving relation between SFR and $\dot{M}_{\rm BH}$, also maintaining a ratio of $\sim 10^{-3}$ for redshifts of $0.5 < z < 2.5$. This was interpreted as a sign that the SFR and $\dot{M}_{\rm BH}$ evolve equivalently throughout cosmic history, in tight relation with one another and with practically no 'lag' between the two, a conclusion supported by Chen et al. (2013), who found an almost linear correlation between the $\dot{M}_{\rm BH}$ and SFR of star forming galaxies for redshifts $0.25 < z < 0.8$.

We can only provide lower limits for the X-ray AGN, but those provide evidence for strong scatter, likely driven by strong AGN variability. Such scatter/variability may well be higher at $z \sim 1$–2 than at lower redshifts. Not only is the BH more active in the X-ray AGN, with accretion rates at least an order of magnitude higher than the stacked sources (compare Tables 1 and 2), but the AGN activity itself may be having an effect on the SFR. We note that our results are consistent with those presented by Lehmer et al. (2013). The stacked sources show an accretion rate/SFR ratio typical of star forming galaxies, while the directly detected sources present a ratio in line with AGN (Fig. 6). This is expected: throughout their lives, galaxies are thought to move above or below the local ratio depending on their AGN activity and SFR.

We note that our results do not depend on the choice of SFR indicator. Particularly, the SFRs obtained from e.g. the radio are in line with those determined with infrared luminosity (~ 1 M$_\odot$ yr^{-1} for $z = 0.4$ and ~ 20 M$_\odot$ yr^{-1} for $z = 2.23$), and are also similar to those derived from Hα. However, we use FIR SFRs because they should be less affected by AGN activity than the radio (and Hα). Even though we excluded radio sources more luminous than 10^{22} W Hz^{-1} (when obtaining radio SFRs), we may still get some AGN contamination. Furthermore, even though SF-related radio emission has its origins in the supernovae of massive stars (whose

lifetimes are comparable to the duration of the SF period), the electrons responsible for the radiation continue emitting for periods of time that reach up to ~ 100 Myr after the original stars exploded. While this 'persistence' of emission depends on factors like the density of the surrounding environment, it means that SFRs from the radio trace time-scales that are longer than those from FIR and Hα.

6 CONCLUSION

We have investigated the relative growth of Hα-selected star-forming galaxies and their supermassive BHs across a redshift range of $0.4 \leq z \leq 2.23$ by making use of the HiZELS sample and the wealth of data available for the COSMOS field. We determined the BH accretion rate of galaxies from their X-ray luminosities and their SFR from their luminosity in the FIR. In this manner, we were able to estimate the $\dot{M}_{\rm BH}$/SFR ratio for typical star-forming galaxies and how that evolves with cosmic time.

Only ~ 3 per cent of the Hα-selected star-forming population are detected in the X-rays as AGN. Our results are in line with the results from the literature: Garn et al. (2010) found that only a few per cent of the Hα emitters at $z = 0.84$ are detected in the X-rays. Sobral et al. (2016) found similar results, with X-ray-detected AGN fractions that varied from 1 per cent to 2–3 per cent for redshifts $0.8 \leq z \leq 2.23$. Our X-ray AGN fractions are 3 per cent for the redshifts $z = 0.4$–1.47 and 2 per cent for $z = 2.23$. This implies that there is no significant evolution of the X-ray AGN fraction with redshift. Our results also complement those from Sobral et al. (2016), who estimated AGN fractions at $z = 0.84$–2.23 for the most luminous Hα emitters and found little to no evolution with redshift.

The FIR SFRs in our sample range from ~ 2 to ~ 40 M$_\odot$ yr^{-1}, from $z = 0.4$ to $z = 2.23$ (Thomson et al. 2016). This is in good agreement with the Hα SFRs (see e.g. Swinbank et al. 2012; Sobral et al. 2014). The $\dot{M}_{\rm BH}$ we obtain are generally a thousandth of the SFRs of the galaxies we studied, in line with results from Lehmer et al. (2013) for star-forming galaxies at $z = 2.23$. The BH accretion rates rise with redshift from $\dot{M}_{\rm BH} \sim 0.004$ M$_\odot$ yr^{-1} at $z = 0.8$ to $\dot{M}_{\rm BH} \sim 0.03$ M$_\odot$ yr^{-1} at $z = 2.23$. The rising of the $\dot{M}_{\rm BH}$ may be steeper until $z = 1.47$. Interestingly, the SFRD evolves in a very similar way to the $\dot{M}_{\rm BH}$, starting to stabilize at around the same redshifts: the $\dot{M}_{\rm BH}$ evolution starts to 'flatten' at $1.47 < z < 2.23$ (e.g. Sobral et al. 2013), something that is supported in the literature, as Aird et al. (2010) has found that the peak of X-ray luminosity density is located at $z = 1.2 \pm 0.1$.

Our $\dot{M}_{\rm BH}$/SFR ratio is observed to have little to no evolution with redshift, being approximately $\sim 10^{-3.3}$ between $z = 0$ and $z = 2.23$. This little to no evolution across redshift suggests that $\dot{M}_{\rm BH}$ and SFRs of our typical star-forming galaxies evolve at similar rates across cosmic time. Our results are thus in good agreement with the ones in the literature. Several authors have noted that the $\dot{M}_{\rm BH}$ and SFR ratio has been independent of cosmic time for the last ~ 10 Gyr, with a value of $\sim 10^{-3.2}$ (see e.g. Hopkins & Beacom 2006; Shankar, Weinberg & Miralda-Escudé 2009; Heckman & Best 2014). It is worth noting that, although our results favour a scenario where the BHs and their host galaxies grow simultaneously as a whole, they do not imply that this is necessarily the case on a galaxy by galaxy basis. Nevertheless, the little to no evolution of $\dot{M}_{\rm BH}$/SFR across cosmic time suggests that the processes that fuel $\dot{M}_{\rm BH}$ and SFR have remained the essentially the same (or correlated) over cosmic time (see, e.g. Heckman et al. 2004; Mullaney et al. 2012). However, understanding and explaining these physical processes in detail (feedback, gas stability and availability) is still a very important open question.

We also find that $\dot{M}_{BH}$/SFR may decline slightly with increasing stellar mass, although very weakly. This specific relation is interesting because the canonical interpretation of the influence of AGN and SF in galaxy evolution is that AGN generally dominate in more massive galaxies whereas in less massive galaxies SF starts playing a more important role. The fact that $\dot{M}_{BH}$/SFR depends so little on galaxy mass could indicate that BH activity and SFR form a combined mechanism for the regulation of galaxy growth, as opposed to simply one mechanism taking over the other at set intervals in time, but this is currently very uncertain.

As for the directly detected sources in the X-rays (X-ray AGN), they show very significant scatter. They seem to deviate from the behaviour of the full population, revealing $\dot{M}_{BH}$/SFR ratios of $> 10^{-3.5}$ to $> 10^{-1.2}$. This is not a surprising result, since AGN activity is highly variable and the BH growth may exceed SFR and vice versa on short time-scales (e.g. Alexander et al. 2008; Targett, Dunlop & McLure 2012).

Future work would need to focus on extending this study to other surveys as well as trying to understand how SF and BH activity might constrain the evolution of the galaxies they happen in. The further use of ALMA to probe gas outflows in AGN and SF galaxies would allow us to get a much more detailed idea of whether these processes affect galaxies differently and let us better understand how AGN and SF influence galaxy growth and themselves.

ACKNOWLEDGEMENTS

REFERENCES

Aird J. et al., 2010, MNRAS, 401, 2531
Alexander D. M. et al., 2003, AJ, 125, 383
Alexander D. M. et al., 2008, AJ, 135, 1968
Best P. N., Kauffmann G., Heckman T. M., Brinchmann J., Charlot S., Ivezić Ž., White S. D. M., 2005, MNRAS, 362, 25
Best P. N., Kaiser C. R., Heckman T. M., Kauffmann G., 2006, MNRAS, 368, L67
Best P. et al., 2013, in Astrophys. Space Sci. Proc. Vol. 37, Thirty Years of Astronomical Discovery with UKIRT. Springer Science+Business Media, Dordrecht, p. 235
Bondi M., Ciliegi P., Schinnerer E., Smolčić V., Jahnke K., Carilli C., Zamorani G., 2008, ApJ, 681, 1129
Bower R. G., Benson A. J., Malbon R., Helly J. C., Frenk C. S., Baugh C. M., Cole S., Lacey C. G., 2006, MNRAS, 370, 645
Brandt W. N., Alexander D. M., 2015, A&AR, 23, 1
Casali M. et al., 2007, A&A, 467, 777
Chabrier G., 2003, PASP, 115, 763
Chen C.-T. J. et al., 2013, ApJ, 773, 3
Davies R. I., Maciejewski W., Hicks E. K. S., Tacconi L. J., Genzel R., Engel H., 2009, ApJ, 702, 114
Delvecchio I. et al., 2014, MNRAS, 439, 2736
Delvecchio I. et al., 2015, MNRAS, 449, 373
Dunn J. P. et al., 2010, ApJ, 709, 611
Elvis M. et al., 2009, ApJS, 184, 158
Ganguly R., Brotherton M. S., 2008, ApJ, 672, 102
Garn T. et al., 2010, MNRAS, 402, 2017
Geach J. E., Smail I., Best P. N., Kurk J., Casali M., Ivison R. J., Coppin K., 2008, MNRAS, 388, 1473
Geach J. E. et al., 2013, MNRAS, 432, 53
Geach J. E. et al., 2014, Nature, 516, 68
Geach J. E. et al., 2016, in press
Genel S. et al., 2014, MNRAS, 445, 175
Griffin M. J. et al., 2010, A&A, 518, L3
Harrison C. M. et al., 2012, ApJ, 760, L15
Heckman T. M., Best P. N., 2014, ARA&A, 52, 589
Heckman T. M., Kauffmann G., Brinchmann J., Charlot S., Tremonti C., White S. D. M., 2004, ApJ, 613, 109
Hopkins A. M., Beacom J. F., 2006, ApJ, 651, 142
Ibar E. et al., 2013, MNRAS, 434, 3218
Karim A. et al., 2011, ApJ, 730, 61
Kormendy J., Ho L. C., 2013, ARA&A, 51, 511
Lehmer B. D. et al., 2007, ApJ, 657, 681
Lehmer B. D. et al., 2013, ApJ, 765, 87
Lehmer B. D. et al., 2016, ApJ, 825, 7
Lilly S. J., Le Fevre O., Hammer F., Crampton D., 1996, ApJ, 460, L1
Lutz D. et al., 2011, A&A, 532, A90
Madau P., Dickinson M., 2014, ARA&A, 52, 415
McNamara B. R., Kazemzadeh F., Rafferty D. A., Bîrzan L., Nulsen P. E. J., Kirkpatrick C. C., Wise M. W., 2009, ApJ, 698, 594
McNamara B. R., Rohanizadegan M., Nulsen P. E. J., 2011, ApJ, 727, 39
Mullaney J. R. et al., 2012, ApJ, 753, L30
Nesvadba N. P. H., Lehnert M. D., Eisenhauer F., Gilbert A., Tecza M., Abuter R., 2006, ApJ, 650, 693
Nesvadba N. P. H., Lehnert M. D., De Breuck C., Gilbert A., van Breugel W., 2007, A&A, 475, 145
Nesvadba N. P. H., Lehnert M. D., De Breuck C., Gilbert A. M., van Breugel W., 2008, A&A, 491, 407
Netzer H. et al., 2007, ApJ, 666, 806
Oliver S. J. et al., 2012, MNRAS, 424, 1614
Oteo I., Sobral D., Ivison R. J., Smail I., Best P. N., Cepa J., Pérez-García A. M., 2015, MNRAS, 452, 2018
Puccetti S., Vignali C., Cappelluti N. et al., 2009, ApJS, 185, 586
Rodighiero G. et al., 2015, ApJ, 800, L10
Rowan-Robinson M., 1995, MNRAS, 272, 737
Schaye J. et al., 2015, MNRAS, 446, 521
Schinnerer E. et al., 2004, AJ, 128, 1974
Schinnerer E. et al., 2007, ApJS, 172, 46
Schmitt H. R., Calzetti D., Armus L., Giavalisco M., Heckman T. M., Kennicutt R. C., Jr, Leitherer C., Meurer G. R., 2006, ApJ, 643, 173
Schnorr Müller A., Storchi-Bergmann T., Riffel R. A., Ferrari F., Steiner J. E., Axon D. J., Robinson A., 2011, MNRAS, 413, 149
Schweitzer M. et al., 2006, ApJ, 649, 79
Scoville N. et al., 2007, ApJS, 172, 1
Shankar F., Weinberg D. H., Miralda-Escudé J., 2009, ApJ, 690, 20
Silk J., Rees M. J., 1998, A&A, 331, L1
Sobral D. et al., 2009a, MNRAS, 398, L68
Sobral D. et al., 2009b, MNRAS, 398, 75
Sobral D., Best P. N., Matsuda Y., Smail I., Geach J. E., Cirasuolo M., 2012, MNRAS, 420, 1926
Sobral D., Smail I., Best P. N., Geach J. E., Matsuda Y., Stott J. P., Cirasuolo M., Kurk J., 2013, MNRAS, 428, 1128
Sobral D., Best P. N., Smail I., Mobasher B., Stott J., Nisbet D., 2014, MNRAS, 437, 3516
Sobral D., Kohn S. A., Best P. N., Smail I., Harrison C. M., Stott J., Calhau J., Matthee J., 2016, MNRAS, 457, 1739
Stanley F., Harrison C. M., Alexander D. M., Swinbank A. M., Aird J. A., Del Moro A., Hickox R. C., Mullaney J. R., 2015, MNRAS, 453, 591
Storchi-Bergmann T., Lopes R. D. S., McGregor P. J., Riffel R. A., Beck T., Martini P., 2010, MNRAS, 402, 819

Swinbank A. M., Sobral D., Smail I., Geach J. E., Best P. N., McCarthy I. G., Crain R. A., Theuns T., 2012, MNRAS, 426, 935
Targett T. A., Dunlop J. S., McLure R. J., 2012, MNRAS, 420, 3621
Thomson A. P. et al., 2014, MNRAS, 442, 577
Thomson A. et al., 2016, ApJ, in press

Tremonti C. A., Moustakas J., Diamond-Stanic A. M., 2007, ApJ, 663, L77
Vasudevan R. V., Fabian A. C., 2007, MNRAS, 381, 1235
Young S., Axon D. J., Robinson A., Hough J. H., Smith J. E., 2007, Nature, 450, 74
Yun M. S., Reddy N. A., Condon J. J., 2001, ApJ, 554, 803

APPENDIX A: FIR SED FITTING
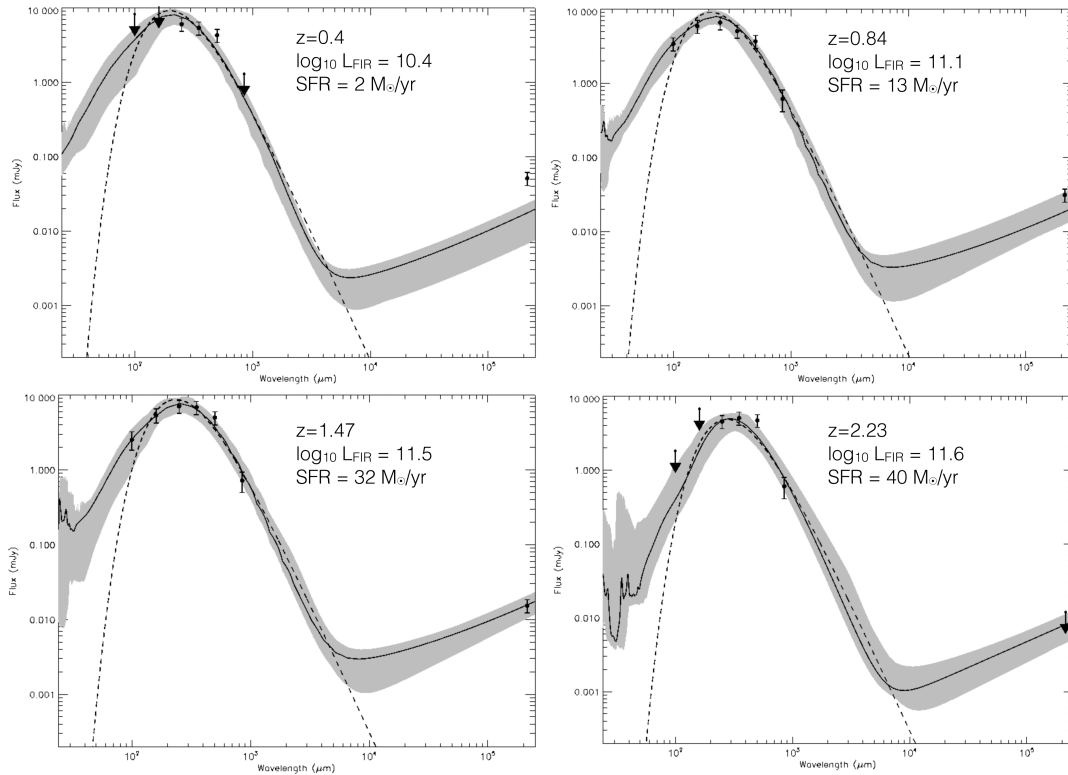
Figure A1. SED fitting for each redshift slice in the FIR bands. The data points were obtained in each band by stacking the entire sample for each redshift using mean statistics. The IR luminosity was estimated by fitting modified blackbody templates to the data points and integrating the best fit between 100 and 850 μm.

APPENDIX B: EVOLUTION OF BHAR AND SFR WITH STELLAR MASS
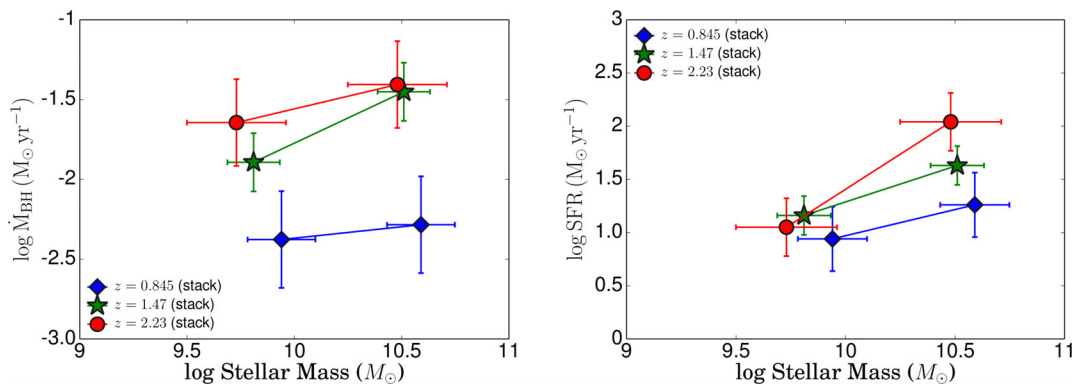
Figure B1. The evolution of the BH accretion rates and SFRs with stellar mass for each of the redshift slices in this work. The SFR grows faster than the BHAR, which results in the overall ratio decreasing with stellar mass.

This paper has been typeset from a TEX/LATEX file prepared by the author.